



NLR-TP-2013-445

Analysis of first AIAA aeroelastic prediction workshop results of oscillating HIRENASD wing

B.B. Prananta, J. Heeg, J. van Muijden, B.J.G. Eussen and
C. Wieseman

Nationaal Lucht- en Ruimtevaartlaboratorium

National Aerospace Laboratory NLR

Anthony Fokkerweg 2

P.O. Box 90502

1006 BM Amsterdam

The Netherlands

Telephone +31 (0)88 511 31 13

Fax +31 (0)88 511 32 10

www.nlr.nl



Executive summary

Analysis of first AIAA aeroelastic prediction workshop results of oscillating HIRENASD wing



Problem area

Aeroelastic prediction methods play an increasingly important role in the design and operation of aircraft. In addition to the traditional role of ensuring avoidance of catastrophic aeroelastic instabilities, aeroelastic prediction methods are applied to exploit aeroelastic deformation for performance gains, to predict the effects of structural flexibility in flight mechanics, and to design flight loads alleviation schemes for increased airframe structural life span.

For aeroelastic validation of prediction methods, the experimental test cases that are open, well-documented and sufficiently rich in measured data are highly limited. Part of the problem is that not only unsteady

aerodynamic data have to be measured, but also structural characteristics of the wind tunnel model and its mounting in the wind tunnel have to be known in quite some detail to unravel the dominant excitations during testing. The Aeroelastic Prediction Workshop (AEPW) addresses several of the available test cases to assess the current status of aeroelastic prediction capabilities. The focus in this report is on the frequency domain unsteady aerodynamic aspects for the HIRENASD test case.

Description of work

In the current report, computational data from several participants of the Aeroelastic Prediction Workshop for the HIRENASD wing test case are compared with each other and

Report no.

NLR-TP-2013-445

Author(s)

B.B. Prananta
J. Heeg
J. van Muijden
B.J.G. Eussen
C. Wieseman

Report classification

UNCLASSIFIED

Date

October 2013

Knowledge area(s)

Aëro-elasticiteit en
vliegtuigbelastingen
Computational Physics en
theoretische aërodynamica

Descriptor(s)

transonic
unsteady
aerodynamics
HIRENASD
aeroelastic prediction workshop

with experimental data. Three test conditions were selected:

- A subsonic case, which should be an easy data point to predict;
- A transonic case at low Reynolds number;
- A transonic case at high Reynolds number.

During the experiment the model is excited close to its natural frequencies. The second bending mode excitation cases were chosen because they were viewed as the simplest ones, having a natural frequency in a range where there is limited influence of the wind tunnel turbulence spectrum. The aeroelastic prediction results are obtained by most participants through excitation with a prescribed motion of the second bending mode. The prediction of results employs the following steps:

1. Modal analysis and extraction of modal data from the finite element model of the wing;
2. Mapping of mode shape data from the finite element model to the aerodynamic surface mesh;
3. Static aeroelastic analysis to determine the fundamental state as starting point for prescribed motion computation;
4. Time-accurate simulation involving deforming grids.

Results and conclusions

Based on comparisons of predicted results for the HIRENASD wing test conditions, a band width of predicted results is obtained. Part of the band width in predicted results can be explained in terms of differences in meshing and in

specific characteristics of the prediction methods. However, the predicted results are in general closer to each other than to the experimental results, even for the subsonic case. Therefore, it is suspected that the exercise is not fully representative for the actual experimental situation. A critical review of the HIRENASD experiment has resulted in five issues that might potentially influence the excitation of the wing motion. Therefore, it is suggested for future experiments to:

- Measure static deformation;
- Measure actual motion;
- Guarantee the dominance of unsteady pressure data for the intended vibration mode;
- Investigate other possible sources of excitation;
- Include test points suitable for analytical verification;
- Fill the unsteady database with more than one frequency per testpoint/mode combination.

Applicability

The current state-of-the-art aeroelastic prediction methods can be applied to available wind tunnel test cases provided that sufficient attention is given to meshing and turbulence modelling issues and to the modal representation of the structural model. Furthermore, the excitation mechanism of the experimental test case should be unambiguously known. The above sketched recommendations for aeroelastic testing are therefore strongly suggested as guidelines for new aeroelastic wind tunnel test campaigns.



NLR-TP-2013-445

Analysis of first AIAA aeroelastic prediction workshop results of oscillating HIRENASD wing

B.B. Prananta, J. Heeg¹, J. van Muijden, B.J.G. Eussen and C. Wieseman¹



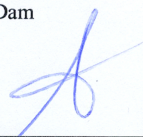
¹ NASA Langley Research Center

This report is based on a presentation held at the International Forum on Aeroelasticity & Structural Dynamics, Bristol, U.K., 24-26 June 2013.

The contents of this report may be cited on condition that full credit is given to NLR and the authors.
This publication has been refereed by the Advisory Committee AEROSPACE VEHICLES.

Customer	National Aerospace Laboratory NLR
Contract number	----
Owner	National Aerospace Laboratory NLR
Division NLR	Aerospace Vehicles
Distribution	Unlimited
Classification of title	Unclassified
	October 2013

Approved by:

Author B.B. Prananta 	Reviewer B.J.G. Eussen 	Managing department A.A. ten Dam 
Date: 23/10/2014	Date: 23/10/2014	Date: 23-10-2014.

Contents

Nomenclature	6
1 Introduction	7
1.1 Use of CFD in aeroelastic analysis	8
1.2 Analysis approach for HIRENASD case	9
2 Selected HIRENASD experiment	9
2.1 Test case selection	10
2.2 Description and processing of experimental data	12
2.3 Finite element model of HIRENASD experiment	13
3 Comparison of oscillating cases	14
3.1 Analysis approach	15
3.2 Processing of computational data	16
3.3 Subsonic case	17
3.4 Transonic nominal lift condition	18
3.5 Transonic low lift condition	19
4 Summary of findings and recommendations for future experiments	19
5 References	20
6 Acknowledgment	21
7 Figures	22

ANALYSIS OF FIRST AIAA AEROELASTIC PREDICTION WORKSHOP RESULTS OF OSCILLATING HIRENASD WING

Bimo Prananta¹, Jennifer Heeg²
Jaap van Muijden¹, Bart Eussen¹, and Carol Wieseman²

¹National Aerospace Laboratory NLR, Amsterdam, The Netherlands

²NASA Langley Research Center, Hampton VA, USA

Keywords: transonic, unsteady, aerodynamics, HIRENASD, aeroelastic prediction workshop

Abstract: This paper presents an analysis of the aeroelastic results for the HIRENASD configuration as contributed to the First AIAA Aeroelastic Prediction Workshop by multiple analysts. The selection of the HIRENASD test case is clarified, a description of the wind tunnel test at ETW is provided, and finite element modelling of the configuration is outlined. The analysis describes the mutual comparison of computational aeroelastic results of the contributors, and also shows the comparison of computational results with experimental data. Differences in computational results of the contributors are analysed in terms of variations in the computational approach, types of methods and meshes. Differences between computational and experimental results are analysed in terms of possible deviations between the actual experimental set-up and assumed computational approach. It is shown that the latter comparison is subject to unresolved uncertainties in the structural modelling and excitation mechanisms.

Nomenclature

Roman symbols

b	Wing span
C_p	Pressure coefficient
C_M	Pitching moment coefficient
C_N	Normal force coefficient
c	Chord
$[c]$	Damping matrix
e	Exponential base number
E	Young's modulus, modulus of elasticity
F_x	Excitation force of mode shape
i	Imaginary unit
k	Reduced frequency
M	Mach number
$[m]$	Generalized diagonal mass matrix
$[m\omega^2]$	Generalized diagonal stiffness matrix
$\{Q(q)\}$	Vector of generalized unsteady aerodynamic force
$\{Q_x(t)\}$	Vector of generalized excitation forces
$\{q(t)\}$	Generalized coordinates
q	Dynamic pressure
Re	Reynolds number
$\{S\}$	Vector of excitation forces
U_∞	Free-stream velocity
$\{x(t)\}$	Displacement in modal space

Greek symbols

α	Angle-of-attack
γ	Ratio of specific heats
Δz	Vertical displacement
ρ	Air density
$[\phi]$	Orthogonal eigenvectors of the undamped structural equations
ω	Frequency, rotational speed

Acronyms

AePW	Aeroelastic Prediction Workshop
BAC	British Aircraft Corporation
CAe	Computational Aeroelasticity
CFD	Computational Fluid Dynamics
CSD	Cross-Spectral Density
DFT	Discrete Fourier Transform
ETW	European Transonic Windtunnel
FEM	Finite Element Model
FRF	Frequency Response Function
HIRENASD	High-Reynolds Number AeroStructural Dynamics
PSD	Power Spectral Density
RWTH	Rheinisch-Westfaelische Technische Hochschule

1 Introduction

Aeroelastic prediction methods play an increasing role in the design and operation of aircraft. In addition to the traditional role of ensuring avoidance of catastrophic aeroelastic instabilities, aeroelastic prediction methods are applied to exploit aeroelastic deformation for performance gains, to predict the effects of structural flexibility in flight mechanics, and to design flight loads alleviation for increased airframe structural lifetime. Reliability of aeroelastic analysis depends on the accuracy of structural dynamics and unsteady aerodynamics modelling. Structural dynamic properties of an aircraft can generally be determined with adequate accuracy through modal updating, based on ground vibration test data. Regarding the aerodynamic modelling, for subsonic flow conditions, linear aerodynamic methods based on lifting surface theory have established their mark as a reliable tool. For transonic flow conditions, however, the situation is less clear. Unsteady aerodynamic analysis methods based on CFD, called Computational Aeroelasticity (CAe), inherit the well-known issues related to physical modelling and numerical solution aspects, e.g. turbulence modelling, shock-wave/boundary-layer interaction, grid dependence, and time integration accuracy. Several preceding studies offered a conclusion that after decades of improved understanding of aeroelasticity, there is still great uncertainty in the ability to predict aeroelastic behaviour using CAe methods. The organisation of the First AIAA Aeroelastic Prediction Workshop (AePW-1) is part of the actions to alleviate this situation. The objective of AePW-1 is to assess state-of-the-art CAe methods, compared to state-of-the-art aeroelastic wind tunnel tests, as practical tools for the prediction of static and dynamic aeroelastic phenomena and responses on available geometries. The workshop was successfully held in April 2012. At that time it was decided that several papers will be dedicated to the analysis of the submitted results of AePW-1.

This paper presents a comparison of submitted computational results with the experimental data for the HIRENASD wing test cases, Ref. (1st AIAA Aeroelastic Prediction Workshop presentations, 2012) (Ballmann, et al., 2008) (Reimer, Boucke, Ballmann, & Behr, 2009). In earlier papers, e.g. Ref. (Heeg & Wiesemann, HIRENASD Comparison Plot, 2012) (Schuster, Chwalowski, Heeg, & Wieseman, 2012), comparison and analysis of the computed pressure coefficients are presented. Here, an assessment will be carried out from an aeroelastic point of view with respect to the results, the underlying methods to generate the results and the characteristics of the measured data. For the prescribed sinusoidal second mode motion of the wing, an analysis of both the pressure distribution, local normal force and local pitching moment along the span will be presented.

From an aeroelastic point of view, it is important that adequate accuracy is maintained at locations where deformation of lifting surfaces occurs. At these locations the energy exchange between aerodynamics and structure is at a maximum. The parameter representing this aspect is known as the generalized aerodynamic force. For the dynamic data, the effects of various features in the pressure distribution on this parameter are analysed. The results of the analyses contribute to the assessment of current state-of-the-art CAe methods and offer recommendations for requirements to be made to future aeroelastic measurements towards a comprehensive validation database of aeroelastic parameters, including unsteady transonic aerodynamics.

1.1 Use of CFD in aeroelastic analysis

Due to the nature of an aeroelastic instability which occurs at relatively low frequency, it is common to express the displacement in a modal space as $\{x(t)\} = [\phi]\{q(t)\}$, where $[\phi]$ are the eigenvectors of the un-damped structural equations and $q(t)$ are the generalised coordinates. The orthogonal property of $[\phi]$ allows the governing aeroelastic equations-of-motion to be written as

$$[m]\{\ddot{q}\} + [c]\{\dot{q}\} + [m\omega^2]\{q\} = \{Q(q)\} + \{Q_x(t)\}, \quad (1)$$

where $\{Q(q)\}, \{Q_x(t)\}$ are the motion-dependent generalised unsteady aerodynamic force and the generalised excitation force, respectively. $[m]$ and $[m\omega^2]$ are diagonal matrices of generalised mass and stiffness. The damping matrix $[c]$ is also diagonal if a proportional damping is assumed.

The obvious reason to apply CFD in an aeroelastic analysis is the presence of nonlinearity in the aerodynamic forces. There are various ways of using CFD in an aeroelastic analysis. The methods can be classified into a direct coupling approach and a surrogate unsteady aerodynamic modelling approach. Methods belonging to the first group include the commonly applied time domain approach and methods with a prescribed periodicity to capture limit cycle oscillation. A direct coupling approach is most suitable for handling genuinely nonlinear aeroelastic problems. The second approach, on the other hand, is usually applied when a linearization is possible, e.g. if one is interested only in the stability property around a specified fundamental state. The fundamental state upon which the linearization is performed can be non-linear with respect to parameters such as Mach number, angle of attack, static deformation, etc. Linear flutter analysis in the frequency domain, such as k and pk -methods, is the prime example. In this case the surrogate model for the unsteady aerodynamics consists of generalised aerodynamic forces for a set of vibration modes and reduced frequencies. Application of CFD for generating frequency domain unsteady aerodynamic data constitutes the current practice in industry.

1.2 Analysis approach for HIRENASD case

The HIRENASD wing case of AIAA AePW-1 is a relevant test case for the application of CFD in generating frequency domain unsteady aerodynamic data for flutter analysis. The HIRENASD cryogenic wind tunnel test in ETW consists of exciting a transport-type wing subjected to transonic flow at or close to its natural frequencies, see Figure 2-3. Two approaches can be carried out to analyse this test case, i.e. by aeroelastic simulations with mechanical excitation or by unsteady aerodynamic simulation with a prescribed motion.

Simulating the experiment as it was executed during the wind tunnel test can be done using Equation (1) with the generalised excitation forces as

$$\{Q_x(t)\} = F_x e^{i\omega_2 t} \{S\} [\phi]^T, \quad (2)$$

where ω_2 is the frequency of the second vibration mode and $\{S\}$ is a vector with mostly zero entries except at the DOF of the finite element model where the excitation force is applied. Referring to Figure 2-3, the entries of $\{S\}$ related to the upper and lower piezo stacks have different sign simulating a moment excitation, see also Ref. (Singh & Castro, 2012). The results of such coupled simulation are aeroelastic responses of the HIRENASD wing. Similar to the experimental time-trace, the data can be processed to obtain transfer functions of the pressure with respect to the motion at the excitation frequency.

Preliminary flutter analyses, Ref. (Prananta, Muijden, & Eussen, 2012), show that the flow conditions of HIRENASD cases are far below the flutter speed. Only relatively small shifts of the frequencies with respect to wind-off are found, signifying a weak aeroelastic coupling at the experimental condition. Another approach besides coupled simulation can therefore be foreseen, i.e. by simply carrying out prescribed sinusoidal second mode motion to the wing. This approach, designated as prescribed motion approach, has been used by most of the AIAA AePW-1 analysts. In the remaining of this paper, the coupled simulation approach will not be considered.

2 Selected HIRENASD experiment

The High Reynolds Number Aero-Structural Dynamics (HIRENASD) experiment, concipiated by the Rheinisch-Westfaelische Technische Hochschule (RWTH) Aachen, was tested in the European Transonic Wind tunnel (ETW) with gaseous nitrogen as the test medium. Wind tunnel model descriptions, testing and experimental data are reported in numerous publications including Refs. (Ballmann, et al., 2011) (Ballmann, et al., 2008) (Dafnis, Korsch, Buxel, & Reimerdes, 2007). Previous computational studies of HIRENASD include Refs. (Reimer, Boucke, Ballmann, & Behr, 2009) (Reimer, Braun, Chen, & Ballmann, 2007) (Neumann, Nitzsche, & Voss, Aeroelastic analysis by coupled non-linear time domain simulation, 2008) (Mavriplis, Yang, Long, & Sitaraman, 2013). Details from some of the AePW computational results can be found in Refs. (Mavriplis, Yang, Long, & Sitaraman, 2013) (Raveh, Yossef, & Levy, 2013) (Chwalowski, Heeg, Wieseman, & Florance, 2013). The HIRENASD configuration was chosen as the first foray of the AePW into aeroelastic systems. Selection of HIRENASD also had the benefit of extending the choice of configurations to include a more airplane-like system.

The HIRENASD configuration has a 34 degrees aft-swept, tapered clean wing, with a BAC 3-11 supercritical airfoil profile. The test article is a semi-span model, ceiling-mounted through a non-contacting fuselage fairing to a turntable, balance and excitation system, shown in Figure 1. Forced motion data was acquired near the structural dynamic modal frequencies using piezoelectric stacks located inside the balance/standoff structure at the wing root.



Figure 1 HIRENASD configuration mounted in ETW

2.1 Test case selection

In this workshop, the organizing committee chose to focus on transonic conditions. Transonic conditions are often considered to be the most critical conditions with regard to aeroelastic phenomena, see Refs. (Edwards, 1991) (Bartels & Sayma, 2009) (Green, et al., 2011). In the transonic range, various flow phenomena can initiate and produce severe aeroelastic issues such as flutter, limit cycle oscillation or buffet. As such, the most significant disagreements among computational results and between experiments and computations are observed. Coupling the criticality and the historically observed discrepancies in the transonic range drew the organizing committee to consider transonic predictions as the necessary starting point for discussion of workshop configurations and cases.

Two cases were selected at a transonic Mach number, Mach 0.8: low Reynolds number at a small positive angle of attack; and one at high Reynolds number at a zero-lift angle of attack. The low Reynolds number case was chosen because the experimental data exhibited a substantial upper surface shock. The high Reynolds number case was chosen to correspond to a case where the pressure distribution might not be fixed in place. It should be mentioned that the high Reynolds number data was obtained with the boundary layer transition strips removed from the wing leading edge; transition point variation might also be a complicating influence.

After initial investigations by several computational teams, a subsonic test case at Mach 0.7 was added to the workshop as a baseline benchmarking point.

The complete HIRENASD experimental data set contains forced excitations of the first and second bending and first torsion modes. The second bending mode excitation cases were chosen because they were viewed as being the simplest ones. The second bending mode frequency was in a range where there is less influence of the wind tunnel turbulence spectrum.

Table 1 Summary of test cases for the HIRENASD wing in AIAA AePW-1

name	flow condition	excitation	remarks
T155	$M=0.7$, $Re=7$ mill, $\alpha=1.5$ deg, $q/E=0.22 \cdot 10^{-6}$	$k_2=0.377$	subsonic
T159	$M=0.8$, $Re=7$ mill, $\alpha=1.5$ deg, $q/E=0.22 \cdot 10^{-6}$	$k_2=0.333$	transonic, high lift
T271	$M=0.8$, $Re=23.5$ mill, $\alpha=-1.34$ deg, $q/E=0.48 \cdot 10^{-6}$	$k_2=0.396$	transonic, low lift

The presence of non-natural frequencies mentioned in Ref. (Ballmann, et al., 2011) by Ballmann issued an investigation into the blade pass frequencies of the ETW compressor. The compressor rotational speed during the selected HIRENASD test points is provided by Dietz (Ref. (Dietz, 2013)) and depicted in Table 2.

Table 2 Tunnel compressor rotational speed in rpm during selected HIRENASD tests

Test	$\omega_{COMPRESSOR}$ [rpm]
T155	489.9
T159	541.8
T271	464

The blade pass frequency is evaluated as $\omega * 36/60$ Hz. It is very interesting to note that the blade pass frequency of the ETW compressor during the HIRENASD experiment turned out to be relatively close to the fifth vibration mode, i.e. the first torsion mode. For the T271 test condition, the blade pass frequency was 278 Hz while the wind-off natural frequency of the HIRENASD wing first torsion mode as predicted using FEM is 276.4 Hz, see section 2.3. This clearly can be a possible source of excitation to the model. For the T155 test condition the blade pass frequency was 294 Hz. This frequency is still relatively close to the first torsion mode of the HIRENASD model. It may be concluded that there is a realistic chance that during the experiment the torsion mode was always excited, regardless of the frequency of the mechanical excitation through the piezo stacks.

An additional complicating factor on pinpointing model excitations is the dependency of vibration mode frequencies on temperature. In Ref. (Schimanski & Hefer, 2000) it is shown that at cryogenic temperatures a significant increase of the vibration mode frequencies of a wind tunnel model can be expected.

It can be suggested that for the future experiments the blade pass frequency of the wind tunnel compressor and its multiples should be analysed carefully against the natural frequencies of the wind tunnel model including possible shifts due to temperature effects.

The flow conditions of the selected test cases of the HIRENASD experiment are in general mild in terms of complexity. The case of T159 representing transonic flow with a nominal lift coefficient has the strongest shock wave boundary layer interaction. Significant flow separation is however not observed in the computational results. Figure 2-2 shows an example of the pressure coefficient and surface flow pattern at the T159 condition. It can be seen that although a significant change in flow direction is observed at the trailing edge, especially at the outer part of the wing, flow separation is not shown. It may be concluded that in terms of flow complexity, the HIRENASD test cases are in general mild.

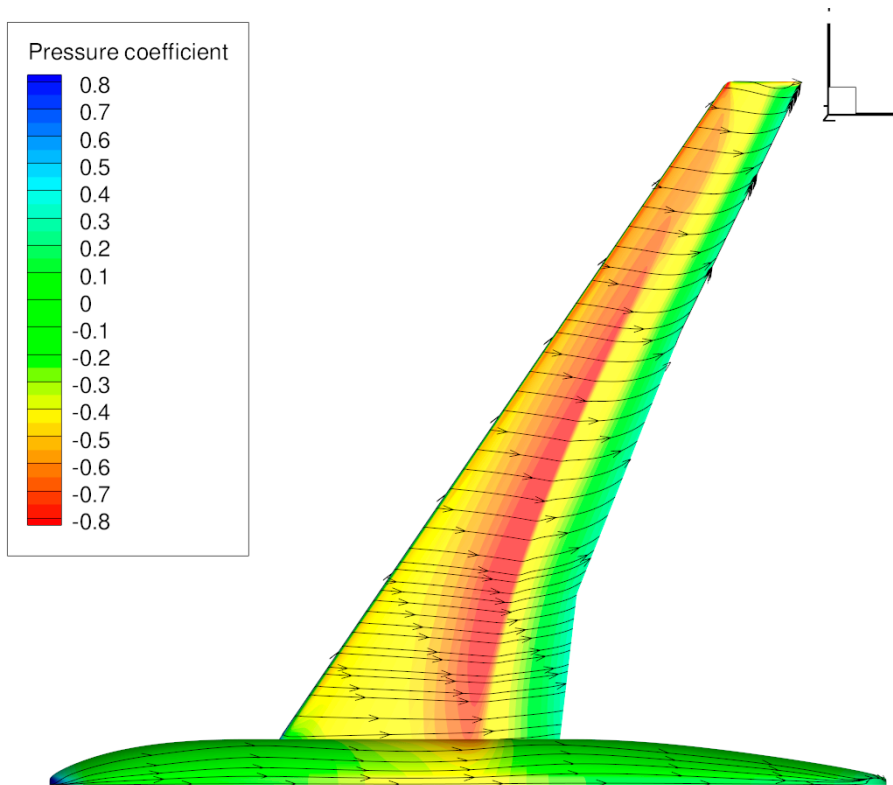


Figure 2-2 Overview of pressure and surface flow pattern for the static aeroelastic reference solution of the T159 case which has strongest shockwave-boundary layer interaction among the HIRENASD test cases. Even at this condition, a flow separation on the upper side of the wing is not observed.

2.2 Description and processing of experimental data

For the workshop comparisons, data from a single test point were used to provide both steady and unsteady data. Data sets with forced oscillations were obtained during the wind tunnel test by sending a low amplitude sinusoidal command, followed by a “rest period”, then followed by a high amplitude sinusoidal command. A subset of the data obtained during the rest period is used to calculate the unforced or steady comparison data. The forced oscillation data was obtained by differential forcing at a specified modal frequency.

The unforced system comparison data utilized at the workshop was the time-averaged (i.e. statistical mean) value taken from the rest periods. A more recent publication of the HIRENASD experimental data has emphasized using the statistical mode to represent the expected values of the unforced system pressure distribution in regions of shock motion. It was demonstrated in Ref. (Heeg & Piatak, Experimental data from the benchmark supercritical wing wind tunnel test on an oscillating turntable, 2013) that representing data in the region of a moving shock with Gaussian process statistics, such as the mean or standard deviations, results in an inaccurate reduction of the shock strength and reshaping the distribution.

The dynamic comparison data for the Aeroelastic Prediction Workshop (AePW) consists of the magnitudes and phases of frequency response functions (FRFs). The FRFs of principal focus were the pressure coefficients, C_p , due to chord-normalized vertical displacement at the location of accelerometer (15,1).

$$C_{p_{NORMALISED}} = C_p / \left(\frac{\Delta z_{ACCELEROMETER (15,1)}}{C_{REF}} \right) \quad (3)$$

The value of Δz at the accelerometer (15,1) for each case is given in Ref. (1st AIAA Aeroelastic Prediction Workshop presentations, 2012). The FRF for each pressure coefficient due to displacement was calculated at the principal frequency of the system response. The results are presented for all chord locations where a pressure measurement was made in the experimental data set.

Fourier domain analysis was performed on the forced excitation portions of the time history data to produce FRFs for each pressure relative to the displacement of the system. The FRFs were formed from PSDs and CSDs, which were computed using Welch's periodogram method. The Fourier coefficients used in computing the PSDs and CSDs were generated using discrete Fourier transform (DFT) analysis of the time histories, employing overlap averaged ensembles of the data sets. The length of the ensembles and the frequency at which the data was extracted were chosen based on statistical analysis of the results of varying the ensemble lengths. The objective in varying the block size is to exactly match the system frequency with a Fourier analysis frequency, and then maximize the number of data blocks to reduce the processing-based uncertainty. The block size for the final analysis was determined by minimizing the standard deviation among the periodograms of the peak of the PSD. In general, this gives a slightly different frequency selection than would be obtained by a selection of the peak value of the PSD. In all cases, a rectangular window was used; the windows were overlapped by 75-95 % of the block size.

2.3 Finite element model of HIRENASD experiment

A geometrically-refined and tuned finite element model (FEM) was analyzed to provide the structural dynamic modes and frequencies for the HIRENASD configuration, see Ref. (Wieseman, Chwalowski, Heeg, Boucke, & Castro, 2013) The original FEM modeled only the wing structure with a cantilevered root boundary condition. The structural dynamic representation was viewed as a potential source of error that would contaminate the aeroelastic response such that the results would not be an accurate reflection of the unsteady aerodynamic simulation capabilities of the flow solvers. Thus, refinements were made to the finite element model for the AePW. These refinements include incorporation of balance, excitation system, instrumentation weights and model cart subcomponents. The FEM was also modified to project the structural outer surface to match the aerodynamic outer mold line used in the aerodynamic grid generation.

Experimental data sets were used for FEM assessment. These data sets were static loadings performed in a laboratory and dynamic excitations obtained with the model installed in the wind tunnel. Comparisons were made between the experimental data and the FEM analysis results including direct comparison of the frequencies, modal assurance criteria applied to the first 5 modes, bending and torsion deflected shape under static loading and node line location.

An assessment of the influence of the changes made to the FEM for the AePW was also performed and documented in Ref. (Wieseman, Chwalowski, Heeg, Boucke, & Castro, 2013). Mode shapes and frequencies from both the original wing-only FEM and the final AePW FEM were used as the bases for unsteady computational aeroelastic simulations. The modal assurance criteria showed improvement in the correlation of the first torsion and fourth bending mode without corruption of the other modes. There was a significant change in the frequency of the second bending mode with minor impact on the other modes. The largest difference in the frequency was due to the addition of the exciter system and balance. The second bending mode node line was shifted inboard and the fourth bending mode was

now captured better in comparison with the experiment. It was demonstrated that neither the static aeroelastic results nor the second bending forced excitation changed significantly with the model updates.

The model and balance were designed to be very stiff, with well-separated vibration modes.

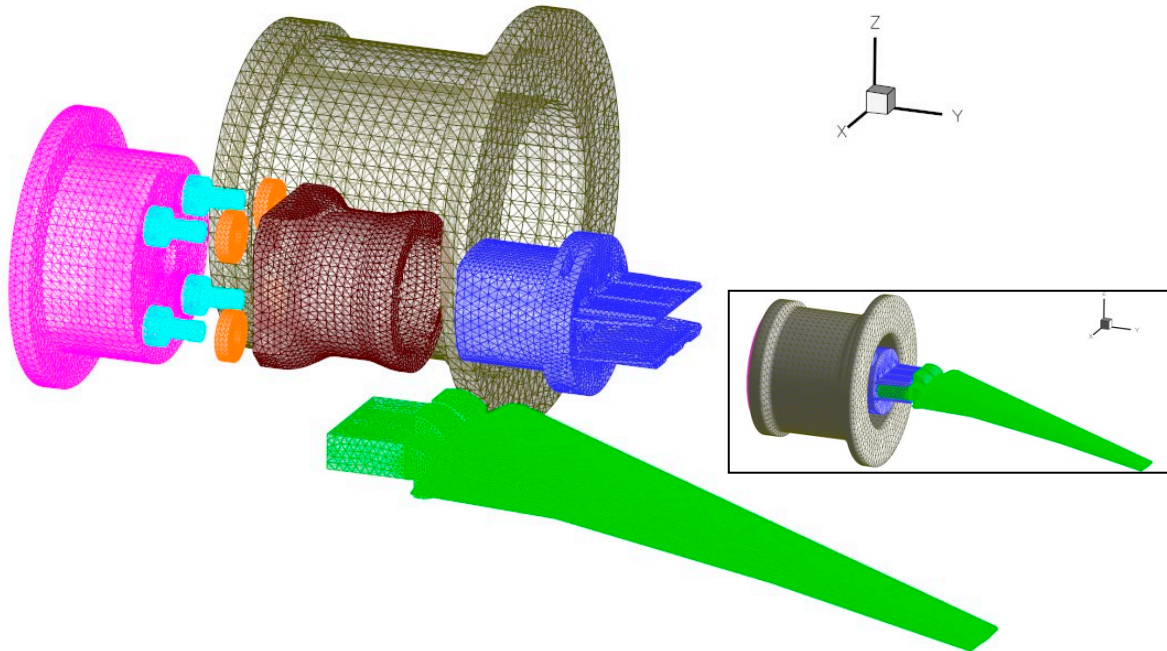


Figure 2-3 Overview of the finite element models showing the components of the HIRENASD experimental setup. The inset shows the models in an assembled state. The light blue and orange coloured components are the model of the piezo linear stack actuators.

3 Comparison of oscillating cases

The present analysis is based on the data submitted by the AePW-1 analysts which have become available in the repository by the end of 2012. Since further post-processing of the data will be carried out, results which do not follow the AePW-1 specified format are excluded from comparison. A summary of the results suitable for comparison is shown in Table 3. Note that the colour code for the analysts has been used consistently throughout the paper. More detailed description of the analysts, designated by code A to K, can be found in the repository of the AIAA AePW-1.

Table 3 Summary of the AIAA AePW-1 results for HIRENASD wing

Code	Method	Turbulence model	Grid type	Grid resolution resolution	Time steps per cycle
A	URANS	$k-\omega$ TNT EARSM	structured	medium	32
B	URANS	$k-\omega$ MSS	structured	coarse	64
C	URANS	$k-\varepsilon$	unstructured	coarse	100
E	URANS	SA	unstructured	coarse, medium	128
F	URANS	SA	unstructured	coarse, medium, fine	64, 128
G	URANS	SA	structured	coarse	64
H	URANS	SA	unstructured	coarse, medium	64
I	Euler-BL	Green's method	structured	coarse	256

J	URANS	SA	unstructured	coarse, medium, fine	64, 256
K	URANS	$k-\omega$ SST	structured	medium	32

It is interesting to note that there is no clear preference on the grid type as used by the analysts, i.e. structured or unstructured, possibly because the configuration is relatively simple. Only one analyst applied a viscous-inviscid Euler-boundary layer interaction method, which is known to be significantly faster in terms of computing time than URANS method. This type of method should be of interest to industries. Another note concerns the results of analyst J. Here, the results for the oscillating wing have been computed starting from the jig shape instead of the statically deformed state.

3.1 Analysis approach

As indicated in section 1.2, most of the participants of the AIAA AePW-1 employ a prescribed modal motion approach to analyse the HIRENASD case. With regard to comparison with experimental data, this approach is valid when the experimental data clearly show a dominant second mode response. Whether this assumption is fully correct will be part of the discussion throughout this paper.

To aid the analysis of the computational results, the steps to perform the analysis of prescribed-motion are listed here:

1. Modal analysis and extraction of modal data from the finite element model. Possible discrepancies introduced at this stage include numerical error in finite element modelling, neglecting the internal damping in the model, possible effects of temperature gradient, etc.
2. Mapping of mode shape data from the finite element model to the aerodynamic surface grid. It is rarely the case that the structural and aerodynamic models match at the fluid-structure interface. Some kind of interpolation method has to be applied which can introduce an error in the computation. Further, the AePW-1 suggests using a subset of surface nodes for interpolation purposes. These nodes can be too coarse for some interpolation methods.
3. Static aeroelastic analysis to determine the fundamental state as starting point for prescribed motion computation. Besides possible errors introduced in the fluid-structure process, in some cases, the flexibility matrix is approximated using a limited number of mode shapes which can introduce an error in the solution. Furthermore, a possible inaccuracy due to differences in the steady flow methods of the different analysts is accumulated in the fundamental state.
4. Time accurate simulation involving deforming grids. This step is possibly the most challenging part of the analysis. Different from the other test cases of AePW-1, the HIRENASD test case requires the use of a deforming grid. A time accurate CFD solution method involving grid deformation would also have many mode-dependent numerical parameters which have to be optimised for a certain type of problem.

In analysing the results of the analysts submitted to the AePW-1, the aforementioned aspects will be used as guideline.

With regard to the parameters employed during the analyses, it is more practical to use the dimensionless parameters. The actual temperatures in various measurement points are different implying that the Young's modulus would also be slightly different leading to different vibration modes. The use of supplied parameters q/E and reduced frequency $k = \omega b/U_\infty$ besides the common aerodynamic parameters $Re_\infty, M_\infty, \gamma, \alpha$ will free the

analyses from many dimensional parameters. Note that q/E is the value based on the flow condition inside the wind tunnel.

In the previous analysis of the AIAA AePW-1 results presented in Ref. (Schuster, Chwalowski, Heeg, & Wieseman, 2012), it has been concluded that good comparison between computational results and experimental data is obtained by the analysts for the static part of the cases. This conclusion is in line with the state of the art of CFD for steady flow, especially for the case without flow separation as has been established in chapter 2. Therefore, the present paper will focus further on the unsteady aerodynamic part of the results.

3.2 Processing of computational data

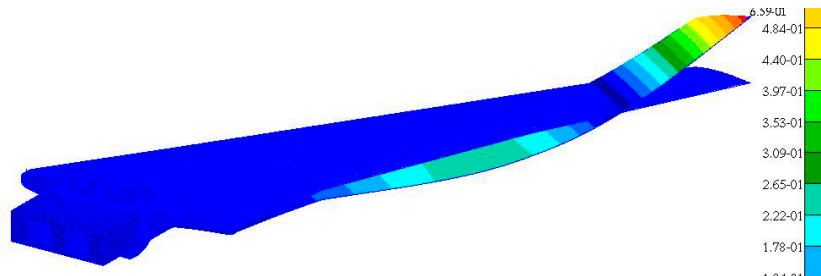
The present paper focusses on the analysis of integrated force and moments. Starting from the FRF of the pressure, the experimental data and the results of AePW-1 analysts are processed into sectional forces and moments and into the generalised aerodynamic forces. The post-processing is facilitated greatly by the submission format of the AePW-1. The identical format of all computational results and the experimental data ensures the consistency of the integrated forces and moments. In this paper, coefficients of normal force $C_N(y) = C_Z(y)$ and pitching moment $C_M(y) = C_{M,y}(y)$ around local quarter chord point are presented. These coefficients are computed by approximating the surface integral with a trapezoidal scheme. Note that only the force component in the z-direction has been taken into account.

Further, the pressure data is also processed into generalised aerodynamic forces as defined in Equation (1). The dimensionless generalised unsteady aerodynamic force for mode i due to excitation of mode 2 is designated as Q_{i2} and is computed as:

$$Q_{i2} = \frac{2}{\rho U_\infty^2} \int_S p \vec{\phi}_i \cdot \vec{dS} \quad (4)$$

The generalised unsteady aerodynamic force can be seen as a pressure-integration, weighted with the magnitude of the vibration mode. In the present analysis the generalised aerodynamic forces for two modes have been calculated, i.e. mode two, second bending mode, and mode five, first torsion mode, see Figure 3-1. The choice for mode two is obvious because it is also the excitation mode. The first torsion mode is also selected because of its significant variation in chord-wise direction which will amplify differences in the chord-wise direction.

$f_2 = 86.5 \text{ Hz}$
second bending



$f_3 = 276.4 \text{ Hz}$
first torsion

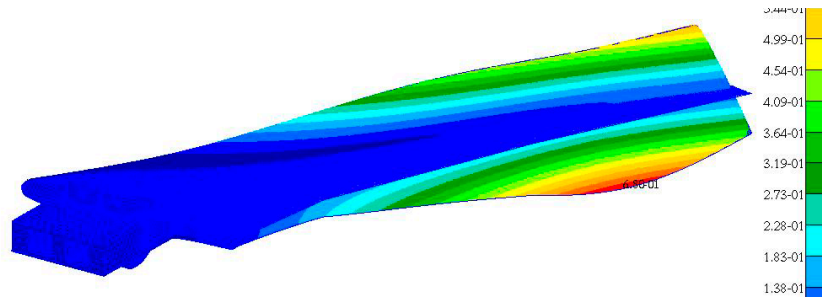


Figure 3-1 Vibration modes of the HIRENASD wing based on the finite element model of the wing only, clamped at its root. The contours represent the distribution of displacements of the vibration modes.

For the computation of the generalised aerodynamic force, the same vibration mode data are used, i.e. those provided by the AIAA AePW-1, to maintain the consistency among the results.

Following the format established in AIAA AePW-1 in normalising the results, all presented quantities are normalised with respect to the amplitude of accelerometer (15,1) of the HIRENASD wing. The actual amplitude for each test case can be found in Ref. (Heeg & Wiesemann, HIRENASD Comparison Plot, 2012).

In the following sections, the HIRENASD cases are discussed. For each case, several plots are made. The main plot contains one result per analyst. If an analyst produced several results, the representative result is the one using medium grid and nominal time step size. Ref. (1st AIAA Aeroelastic Prediction Workshop presentations, 2012) provides a clear definition on the classification of fine, medium and coarse grid sizes and other definitions.

3.3 Subsonic case

The flow condition for the T155 case is completely subsonic. It may be assumed that concurring to the established state of the art of CFD, the analysis should perform well for this case.

Figure 6-1 and Figure 6-2 present the distribution of local normal force and local pitching moment coefficients along the span, respectively. For the local normal force coefficient, the real part clearly shows good agreement among the computational results and between computational results and the experiment. Less satisfactory agreement is obtained for the imaginary part between computational results and the experimental data. Good agreement is however obtained between most of the computational results. One result of analyst J seems to show differences compared to the rest. To look whether this is caused by grid effects a plot is made for various grid densities for analysts F and J and shown in Figure 6-3. While the results of analyst F do not show significant differences for various grid densities, the results of analyst J show significant differences and, moreover, a wrong tendency towards finer grids. Using the jig shape instead of the statically deformed shape proves to be a source of disturbances here.

To examine the differences between computational results and experimental data for the imaginary part of the local normal coefficient, additional plots of the pressure coefficients are made for section 3 and 4 and are shown in Figure 6-4 and Figure 6-5, respectively. It can be seen that differences are observed at the upper surface and to a lesser extent at the lower surface for the whole chord. This suggests that the differences are of systematic nature. Such differences can originate from a disagreement with regard to the motion of the wing. While the computational results are obtained with an excitation of one frequency and one vibration mode, the actual wing motion during the experiment might contain significant contributions

from other vibration modes. In addition, the real part of the experimental pressure shows some spikes. These spikes indicate regions of increased dynamic response due to aerodynamic fluctuations.

The comparison of the local pitching moment coefficients show a less satisfactory agreement with the experimental data for the real part, see Figure 6-2. However, the magnitude of the pitching moment is relatively small, so it would be sensitive to the irregularities in the experimental data observed in the pressure plots. The agreement between computational results can be considered satisfactory.

Comparisons of the generalised aerodynamic forces are presented in Figure 6-6 and Figure 6-7 for Q_{22} and Q_{52} , respectively. The value of the generalised aerodynamic forces are also normalised using the amplitude of the accelerometer (15,1). The generalised aerodynamic forces computed using doublet lattice method of NASTRAN are included for reference. The observation with regard to comparison of local aerodynamic force coefficient is also observed for Q_{22} that the real part shows good agreement between the computational results and the experimental data, with less good agreement for the imaginary part.

Based on the previous discussions, it may be concluded that for this subsonic test case in general the computational results compare well with the experiment. Some differences, however, remain. Besides the possible numerical modelling issues, the differences may be attributed to the mismatch in the input data between the computational setup and the experimental condition, e.g. the reduced frequency, the mode shape, etc. It may also be noted that some parameters selected during post-processing of the data can also influence the FRF results.

3.4 Transonic nominal lift condition

The HIRENASD case designated by T159 represents a transonic case with nominal lift. A shock wave exists at the upper side of the wing almost along the whole span, see Figure 2-1. The specified amplitude of oscillation generates relatively small perturbation on the flow leaving the shockwave present during the whole period of oscillation. The preliminary study in Ref. (Prananta, Muijden, & Eussen, 2012) confirms the relatively small effects of varying amplitude to the unsteady pressure. This means that in terms of complexity of the flow condition, the HIRENASD T159 should be well within reach of state-of-the-art CFD-methods.

Figure 6-8 presents the comparison of local normal force coefficient along the span for all analysts, one representative result per analyst. Two results from analyst B and E seem to divert from other results and can be considered as outliers. It is interesting to note that the results employing the simplified method of viscous-inviscid interaction of analyst I seem to follow the trend of the other computational results for the integrated lift coefficient. When the detailed pressure coefficients are examined, it is noticed that this method overpredicts the upper shock magnitude and predicts its location further aft than the other analysts at every span station. This is an example where the integration process eliminates essential details of the flow calculations. The integrated moment coefficient, however, does indicate that this analysis is not in line with the other cases. The experimental results reside within the band formed by the computational results. The agreement among the computational results can be considered satisfactory. Figure 6-9 shows the impact of grid density on the local normal force results. Most results lie reasonably close in a narrow band. Again, participant J shows a rather remarkable variation with mesh refinement.

The comparison of local moment coefficient along the span as presented in Figure 6-10 shows a much broader spread of the computational results. In addition to the small magnitude of the local pitching moment coefficient, for the transonic case, it is influenced strongly by the predicted location of the shock wave. The different behaviour of results from the simplified method of viscid-inviscid interaction (analyst I) is clearly seen, especially at the outer part where the shock wave is strongest. It may be expected that grid density significantly affects the location of the shock wave. Figure 6-11 isolates the computational results of analysts who performed computation on various grid densities. This plot suggests that better agreement to the experiment is obtained using a finer grid density.

Comparisons of the generalised aerodynamic forces are presented in Figure 6-12 for Q_{22} and in Figure 6-13 for Q_{52} . Confirming the discussion on the local normal force coefficient, ignoring the outliers, the agreement among the computational results as well as between computational results and experimental data is good. Similar conclusion with regard to local pitching moment coefficient may be drawn for the comparison of Q_{52} .

3.5 Transonic low lift condition

The HIRENASD case T271 is similar to the T159, except that the wing lift is very low, close to zero. For linear methods like the doublet lattice of NASTRAN, the unsteady aerodynamic part does not depend on static parameters such as angle of attack. Differences in the unsteady aerodynamic data between test case T159 and T271 can therefore be attributed to nonlinear effects, besides the Reynolds number effects. Due to the weak shockwave in this test case, the shockwave may disappear during part of the period of oscillation. Therefore this test case may be considered to be more difficult compared to the T159 case.

Comparison of the local normal force coefficient along the span is shown in Figure 6-14. Again the results of analyst B seem to be an outlier. Good agreement is obtained among the computational results. Similar to the T155 case, the agreement of the real part of the local normal force coefficient is much better than for the imaginary part. The afore-mentioned existence of a weak shock wave may contribute to this.

Comparison of the local pitching moment coefficient along the span is depicted in Figure 6-15. Less satisfactory agreement is obtained among the computational results. This time both real and imaginary parts of the local pitching moment coefficient show less satisfactory agreement. The pitching moment coefficient is influenced strongly by the resolution of the shock wave motion. Due to the low lift coefficient of the configuration relatively similar strength of the shockwave can exist both at the upper and lower side of the wing.

Figure 6-16 and Figure 6-17 present the generalised aerodynamic forces of Q_{22} and Q_{52} , respectively. The weighting factor related to the shape of mode 2 and mode 5 more or less represents the normal force and pitching moment. The latter is with respect to the nodal line of the mode 5 which is about mid chord. Therefore similar conclusion may be drawn for the generalised aerodynamic forces.

4 Summary of findings and recommendations for future experiments

The following uncertainties have been identified in the current paper that may play a role in the comparison of simulated and experimental results:

1. The subsonic case T155 is not correctly predicted by the CAe/CFD methods. This case should be captured well using CFD. Therefore a significant contribution of other vibration modes may have occurred.
2. Possible unwanted excitation of higher modes through nearly coinciding blade pass frequencies.
3. The cryogenic temperature has a significant effect on wind tunnel model vibration frequencies.
4. The CFD approach using a single prescribed sinusoidal mode of the model may not capture the actual motion of the experiment in the wind tunnel.
5. In the transonic case, the mesh density seems to determine the quality of the comparison with experiment, although the trends shown by some analysts are not understood.

It has to be mentioned that the HIRENASD experiment is certainly a significant advancement in terms of validation data for unsteady aerodynamic analysis methods. The strive to have unsteady aerodynamic data about a wing oscillating in flexible mode is noble and should be encouraged for continuation. However, since the HIRENASD experiment is relatively new, some aspects may need improvement in the future.

Based on the results and findings of the present study, recommendations for the definition of requirements for future experiments can be formulated as follows:

1. The static deformation of the model has to be measured, at least the bending and torsional deformation data along the span.
2. The actual motion of the model during the experiment has to be measured accurately, or the experiment has to allow better control over the prescribed motion during the test.
3. An experimental approach should be devised to ensure that the unsteady pressure data for the intended vibration mode is significantly and undisputably dominant compared to other unsteady data.
4. Possible sources of excitations besides the intended one should be carefully considered, such as the blade pass frequency, buffet, etc.
5. Enough reference data should be measured at test points where analytical methods can reproduce correctly, e.g. subsonic condition, small amplitude, etc.
6. For an aeroelastic validation purpose the experimental unsteady database has to span more than one frequency per testpoint/mode combination.

5 References

- [1] "1st AIAA Aeroelastic Prediction Workshop presentations," NASA, 2012. [Online]. Available: https://c3.nasa.gov/dashlink/static/media/other/AePW_likeAB_main_v2.htm.
- [2] J. Ballmann, A. Dafnis, H. Korsch, C. Buxel, H. G. Reimerdes, K. H. Brakhage, H. Olivier, C. Braun and A. Baars, "Experimental Analysis of High Reynolds Number Aero-Structural Dynamics in ETW," in *AIAA Paper 2008-841*, 2008.
- [3] L. Reimer, A. Boucke, J. Ballmann and M. Behr, "Computational Analysis of High-Reynolds Number Aero-structural dynamics HIRENASD," in *IFASD 2009*, Seattle, 2009.
- [4] J. Heeg and C. Wiesemann, "HIRENASD Comparison Plot," in *AIAA Aeroelastic Prediction Workshop 1*, Honolulu, 2012.

- [5] D. Schuster, P. Chwalowski, J. Heeg and C. Wieseman, "Summary of data and findings from the first aeroelastic prediction workshop," in *Seventh International Conference on Computational Fluid Dynamics*, Big Island, Hawaii, 2012.
- [6] B. Singh and J. Castro, "HIRENASD Analysis Using MSC NASTRAN OpenFSI and CFD++," in *1st AIAA Aeroelastic Prediction Workshop*, Honolulu, Hawaii, 2012.
- [7] B. Prananta, J. v. Muijden and B. Eussen, "Transonic unsteady aerodynamic analysis of HIRENASD wing oscillating in flexible modes," in *AIAA 1st Aeroelastic Prediction Workshop, NLR-TP-2012-476*, Honolulu, Hawaii, 2012.
- [8] J. Ballmann, A. Boucke, B.-H. Chen, L. Reimer, M. Behr, A. Dafnis, C. Buxel, S. Buesing, H.-G. Reimerdes, K.-H. Brakhage, H. Olivier, M. Kordt, J. Brink-Spalink, F. Theurich and A. Büscher, "Aero-Structural Wind Tunnel Experiments with Elastic Wing Models at High Reynolds Numbers (HIRENASD-ASDMAD)," in *AIAA paper 2011-0882, 49th Aerospace Sciences Meeting, Jan. 2011*, Orlando, FL., 2011.
- [9] A. Dafnis, H. Korsch, C. Buxel and H.-G. Reimerdes, "Dynamic response of the HIRENASD elastic wing model under wind-off and wind-on conditions," in *IFASD paper 2007-073*, Stockholm, SE, 2007.
- [10] L. Reimer, C. Braun, B.-H. Chen and J. Ballmann, "Computational Aeroelastic Design and Analysis of the HiRENASD Wind Tunnel Wing Model and Tests," in *IFASD*, Stockholm, SE, 2007.
- [11] J. Neumann, F. Nitzsche and R. Voss, "Aeroelastic analysis by coupled non-linear time domain simulation," in *RTO report RTO-MP-AVT-154*, Loen, 2008.
- [12] D. Mavriplis, Z. Yang, M. Long and J. Sitaraman, "Results using NSU3D for the first aeroelastic prediction workshop," in *51st AIAA Aerospace Sciences Meeting*, Grapevine, TX, 2013.
- [13] D. Raveh, Y. Yossef and Y. Levy, "Flow simulations for the first aeroelastic prediction workshop using the EZNSS Code," in *AIAA Paper 2013-0787*, 2013.
- [14] P. Chwalowski, J. Heeg, C. Wieseman and J. Florance, "FUN3D analyses in support of the first aeroelastic prediction workshop," in *AIAA Paper 2013-07854*, Grapevine, TX, 2013.
- [15] J. Edwards, "Technical evaluation report on 1991 specialists meeting on transonic unsteady aerodynamics and aeroelasticity," in *AGARD CP-507*, 1991.
- [16] R. Bartels and A. Sayma, "Computational aeroelastic modelling of airframes and turbomachinery: progress and challenges," in *AIAA Paper 2009-1360*, 2009.
- [17] B. Green, R. Czerwiec, C. Cureton, C. Lillian, S. Kernazhitskiy, T. Eymann, J. Torres, K. Bergeron and R. Decker, "Evaluation of flow solver accuracy using five simple unsteady validation cases," in *AIAA Paper 2011-29*, 2011.
- [18] G. Dietz, *Personal communication with B. Eussen*, 2013.
- [19] D. Schimanski and G. Hefer, "Recent Aspects of High Reynolds Number Data Quality and Capabilities at the European Transonic Windtunnel," in *AIAA paper 2000-0292*, Reno, NV, 2000.
- [20] J. Heeg and D. Piatak, "Experimental data from the benchmark supercritical wing wind tunnel test on an oscillating turntable," in *AIAA Paper 2013-1801*, 2013.
- [21] C. Wieseman, P. Chwalowski, J. Heeg, A. Boucke and J. Castro, "Structural dynamics modelling of HIRENASD in support of the aeroelastic prediction workshop," in *AIAA Paper 2013-1801*, 2013.
- [22] J. Neumann and M. Ritter, "Computational Analysis of High Reynolds Number

Aerostructural Dynamics (HiReNASD) Experiments,” in *IFASD paper 2009-132*, Seattle, WA, 2009.

- [23] J. Ballmann, A. Boucke, C. Dickopp and L. Reimer, “Results of dynamic experiments in the HIRENASD project and analysis of observed unsteady processes,” in *IFASD paper 2009-103*, Seattle, WA, 2009.

6 Acknowledgment

The work presented is partly funded by the Netherlands Ministry of Defence, through the LCK2013/2016 programme. The authors gratefully acknowledge the AePW team, particularly the HIRENASD analysts and the AePW Organizing Committee.

7 Figures

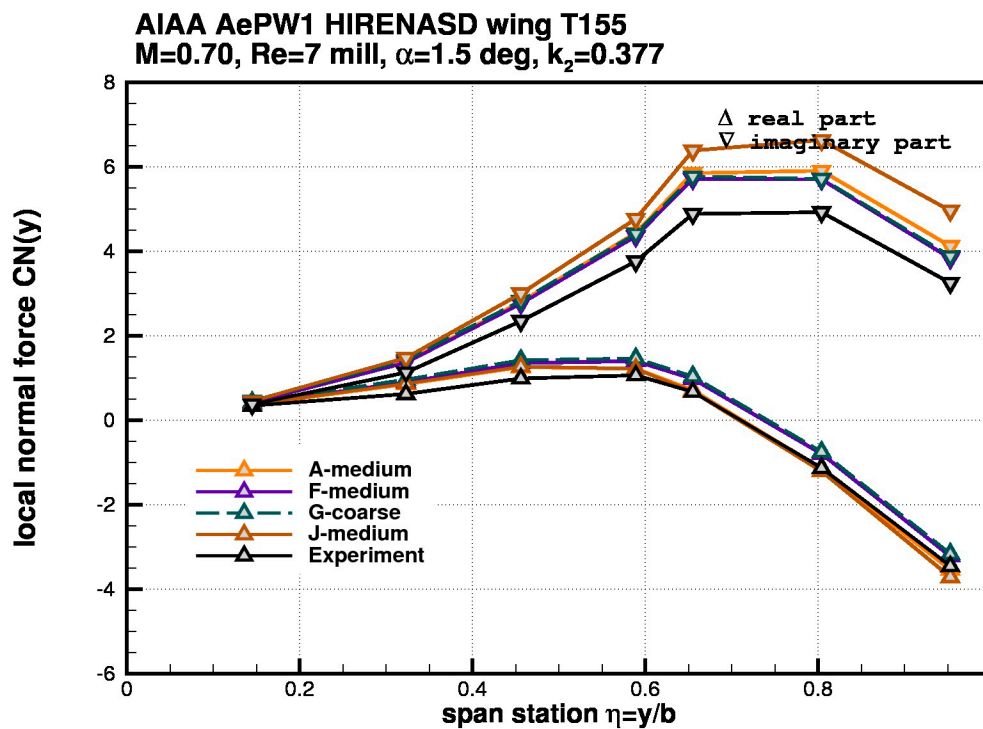


Figure 6-1 Comparison of computational results and experimental data for the representative results of all analysts, see also Table 1 (T155_CN_med.jpg)

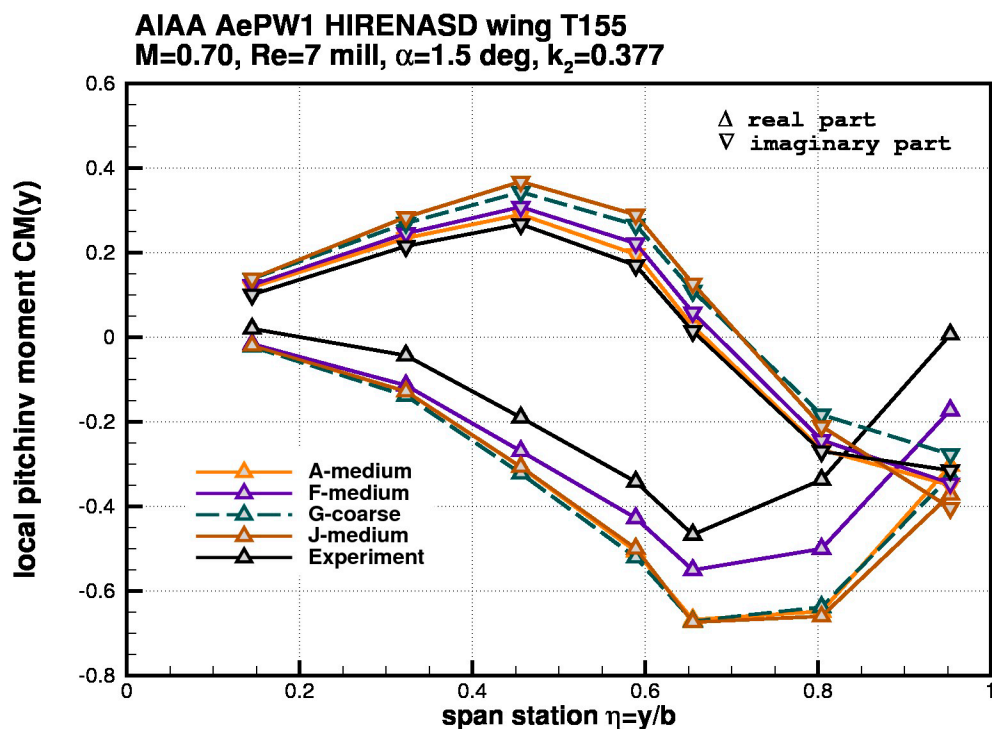


Figure 6-2 Comparison of computational results and experimental data for the representative results of all analysts, see also Table 1 (T155_CM_med.jpg)

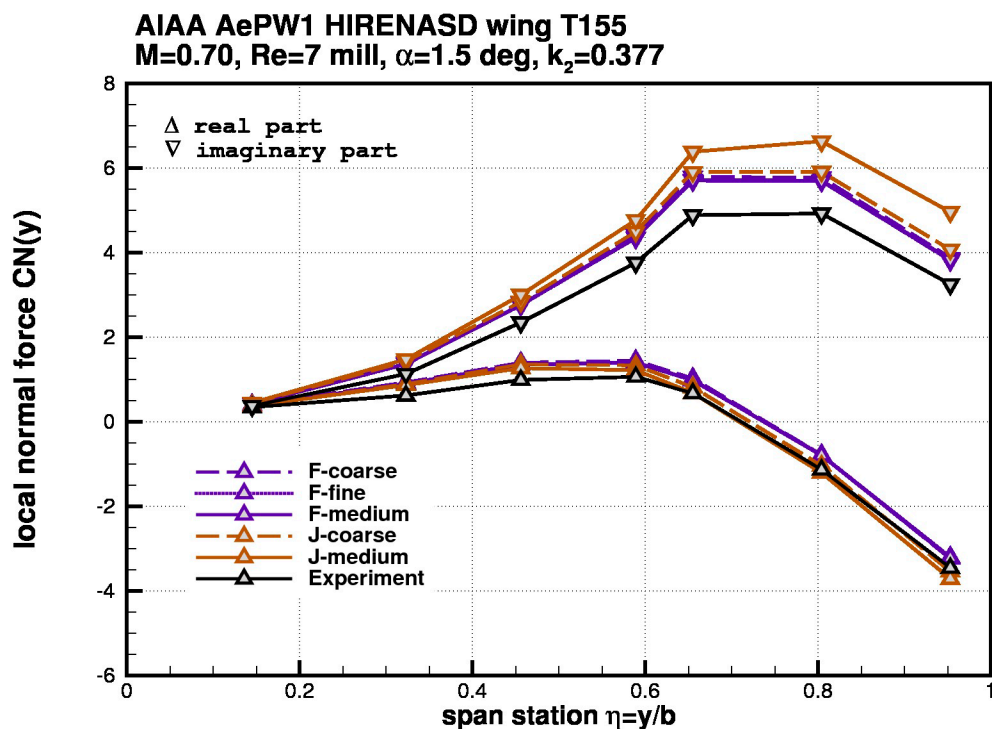


Figure 6-3 Comparison of computational results and experimental data for various grid densities, see also Table 1 (T155_CN_grd.jpg)

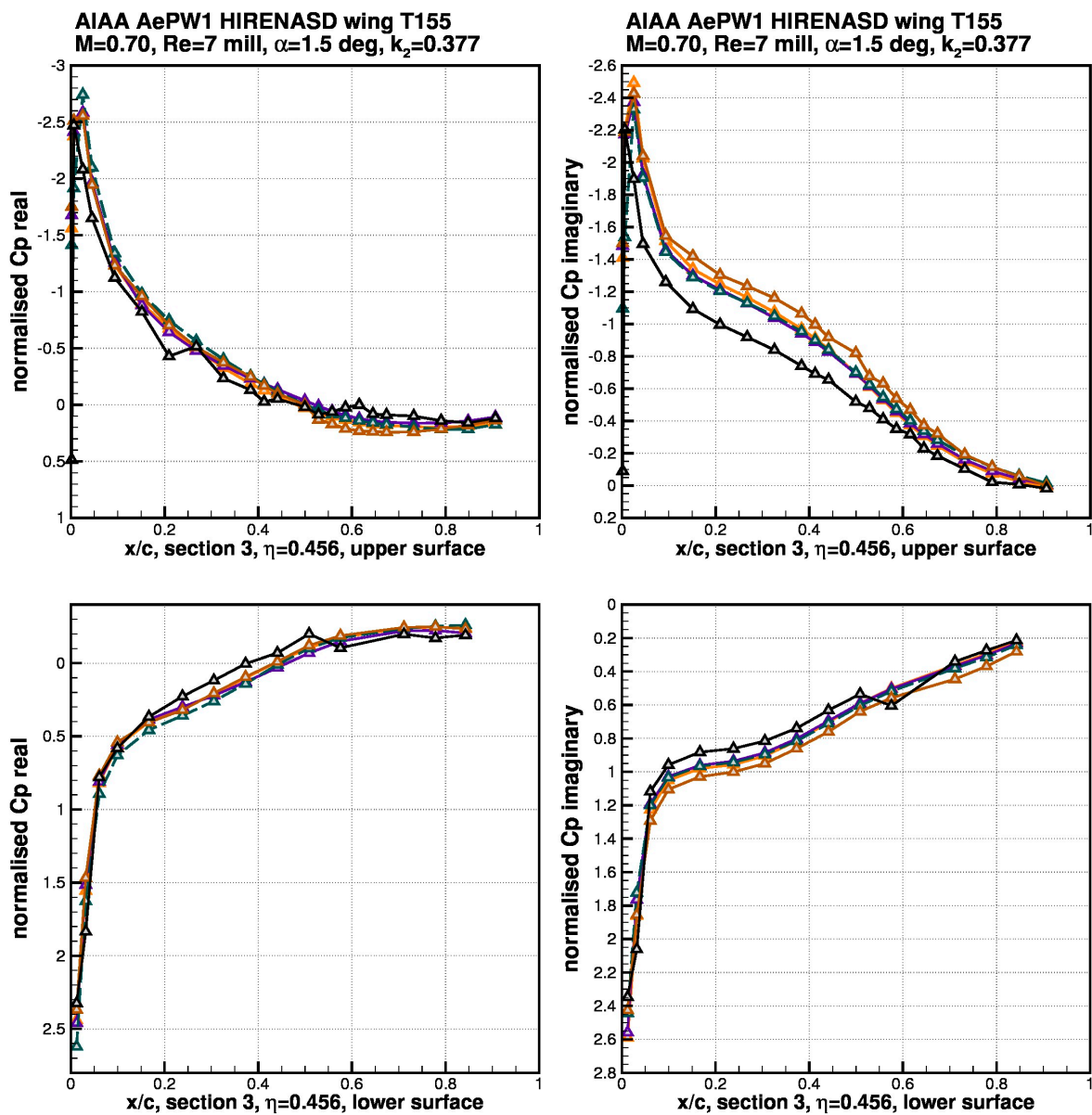


Figure 6-4 Comparison of computational results and experimental data for the representative results of all analysts, see also Table 1 (T155S3_med.jpg)

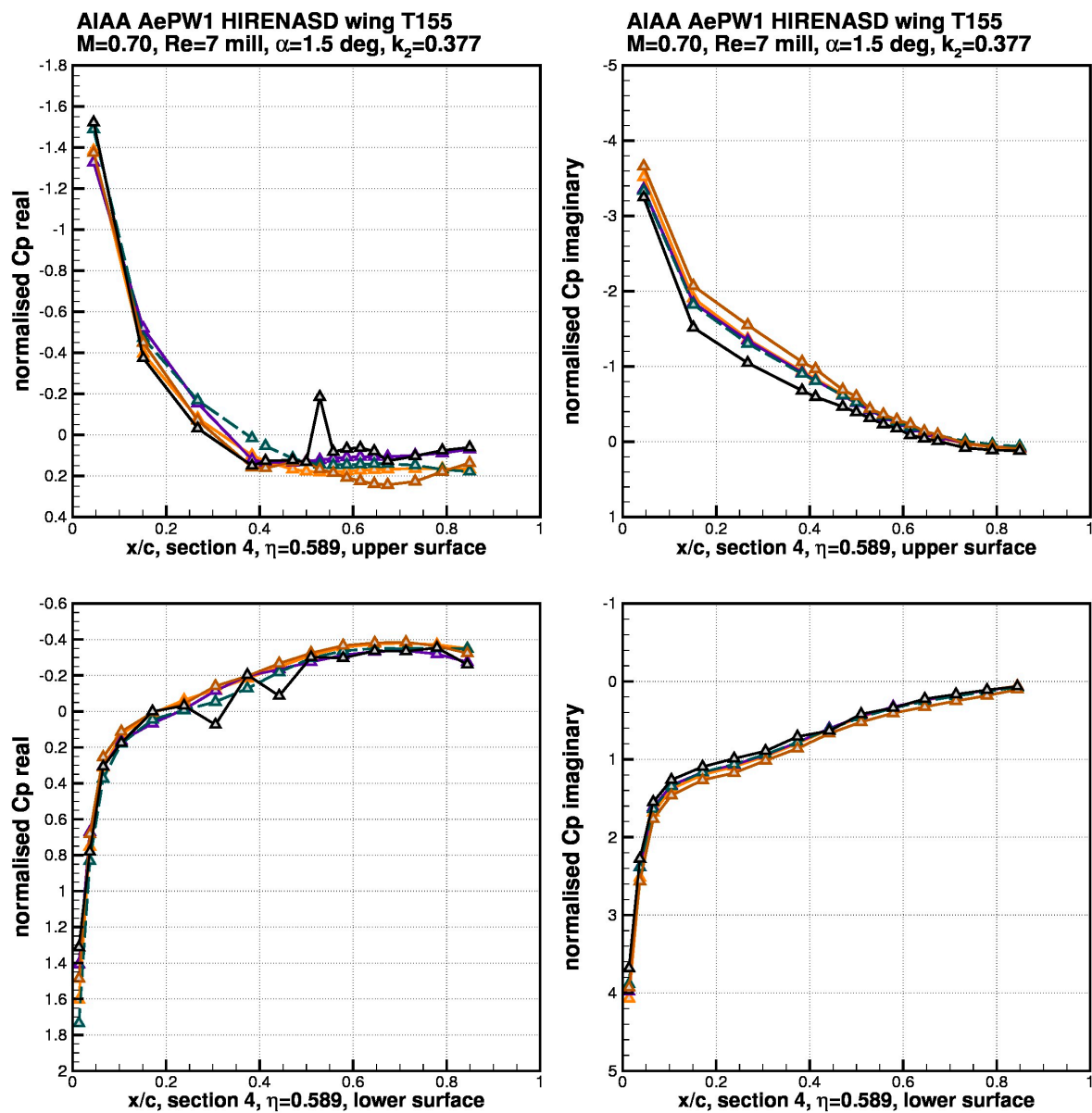


Figure 6-5 Comparison of computational results and experimental data for the representative results of all analysts, see also Table 1 (T155S4_med.jpg)

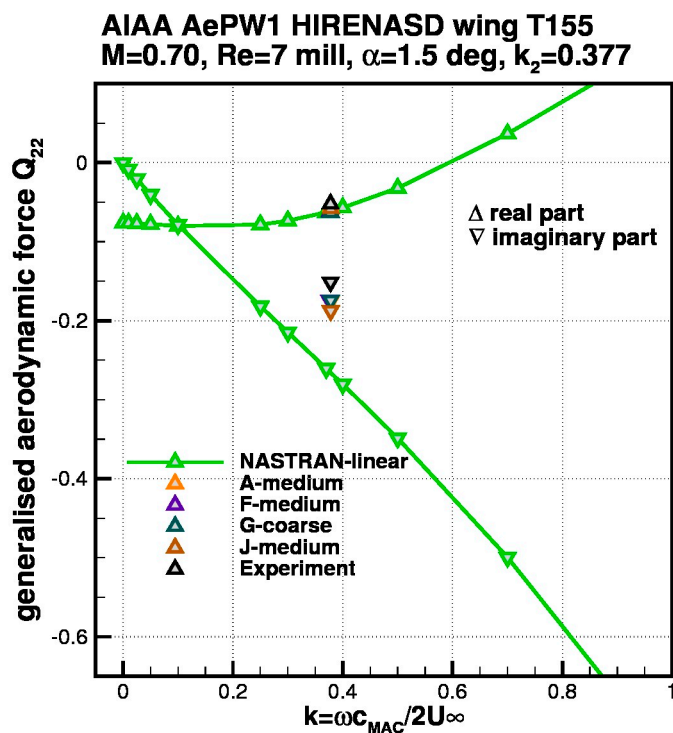


Figure 6-6 Comparison of computational results and experimental data for the representative results of all analysts, see also Table 1 (T155_Q22_med.jpg)

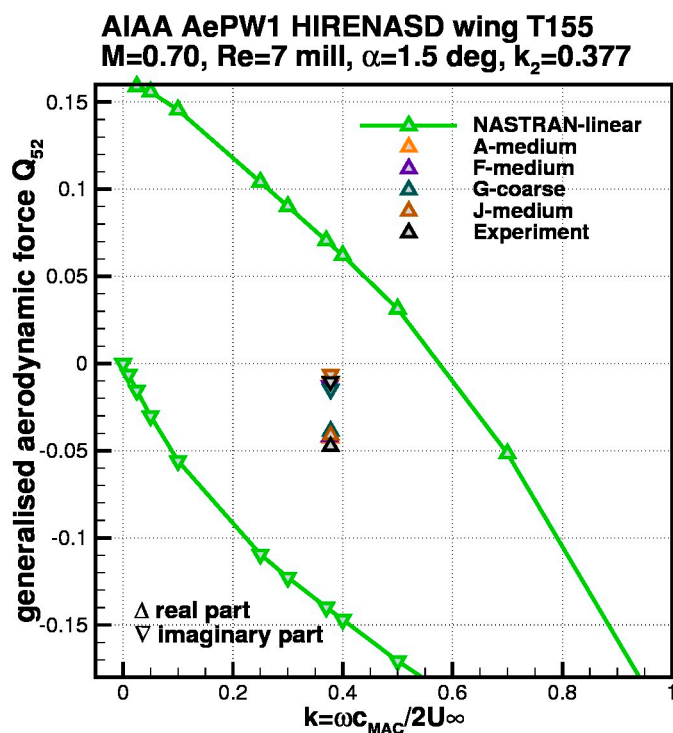


Figure 6-7 Comparison of computational results and experimental data for the representative results of all analysts, see also Table 1 (T155_Q52_med.jpg)

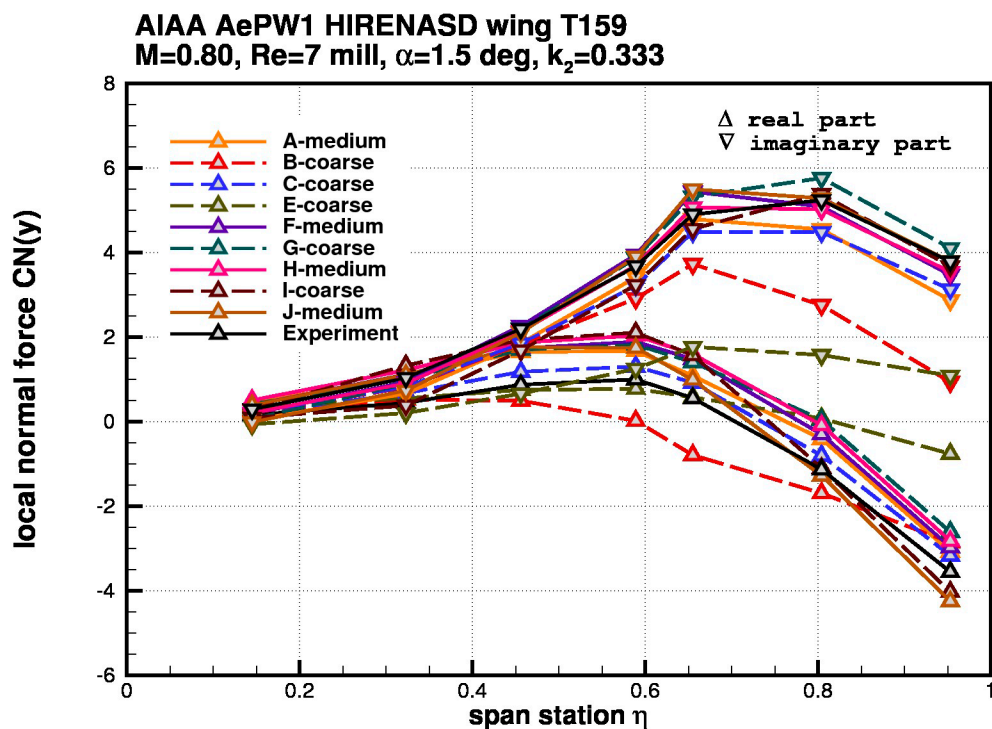


Figure 6-8 Comparison of computational results and experimental data for the representative results of all analysts, see also Table 1 (T159_CN_med.jpg)

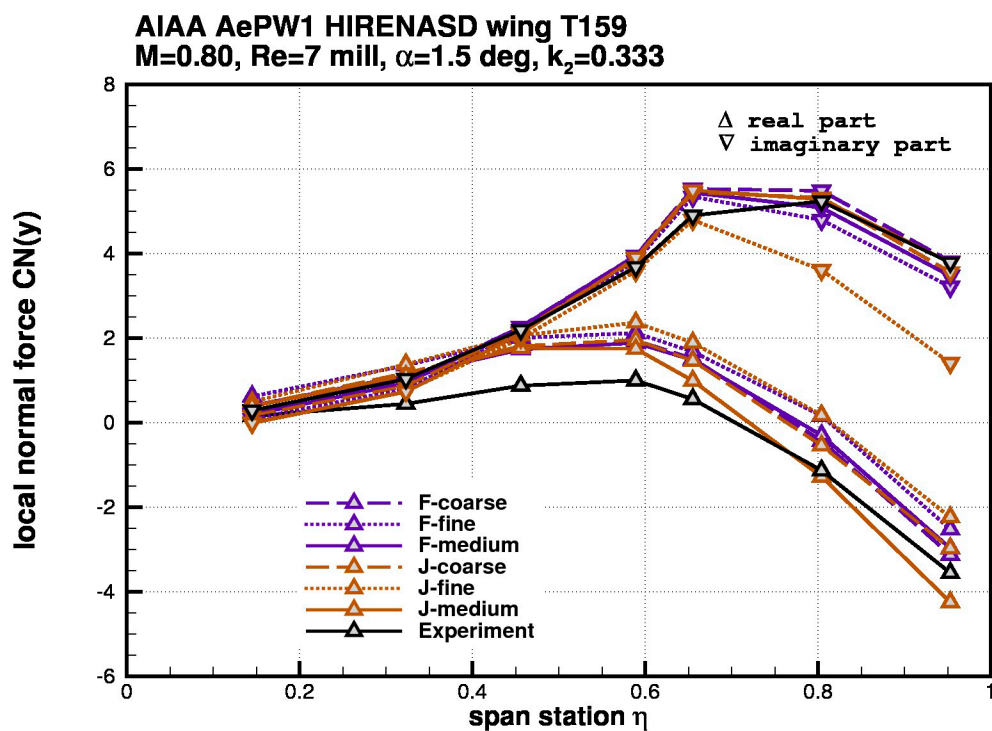


Figure 6-9 Comparison of computational results and experimental data for various grid densities, see also Table 1 (T159_CN_grd.jpg)

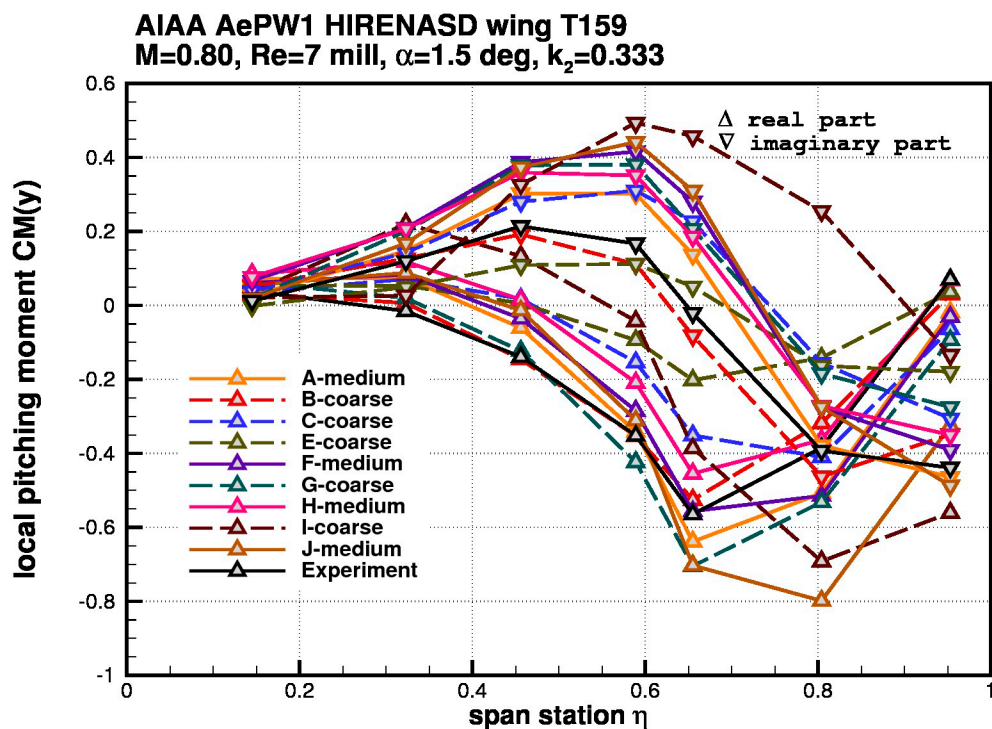


Figure 6-10 Comparison of computational results and experimental data for the representative results of all analysts, see also Table 1 (T159_CM_med.jpg)

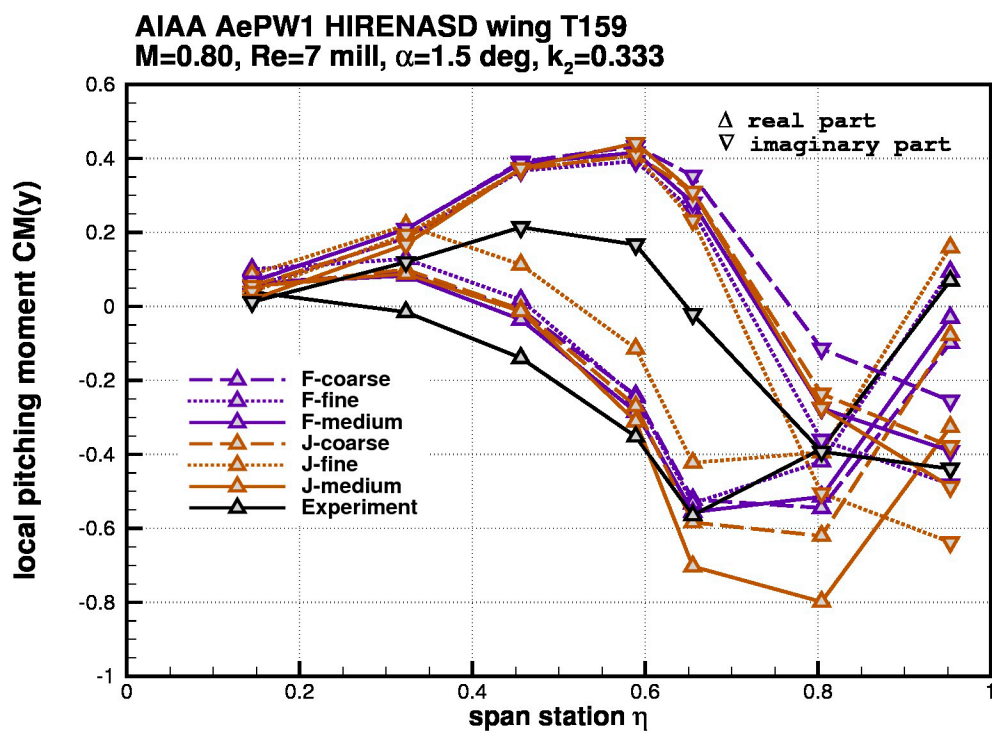


Figure 6-11 Comparison of computational results and experimental data for various grid densities, see also Table 1 (T159_CM_grd.jpg)

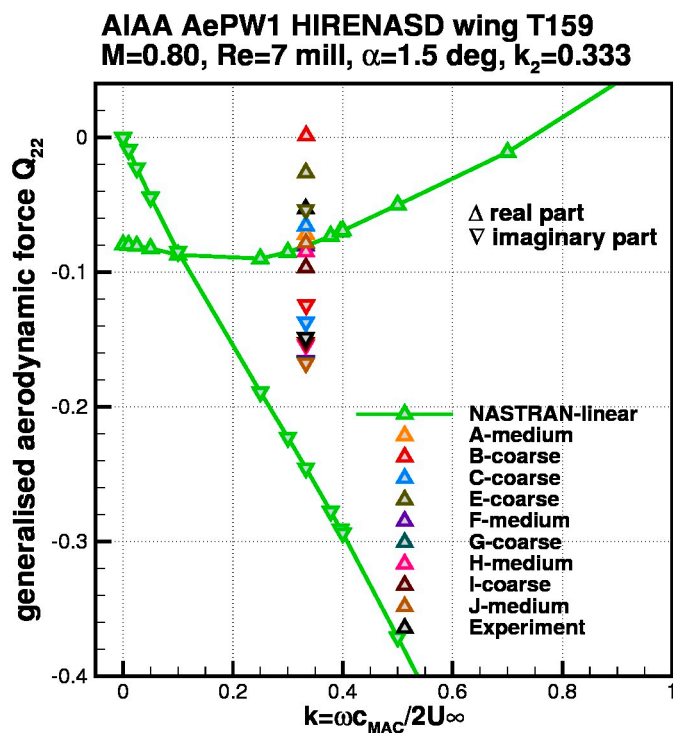


Figure 6-12 Comparison of computational results and experimental data for the representative results of all analysts, see also Table 1 (T159_Q22_med.jpg)

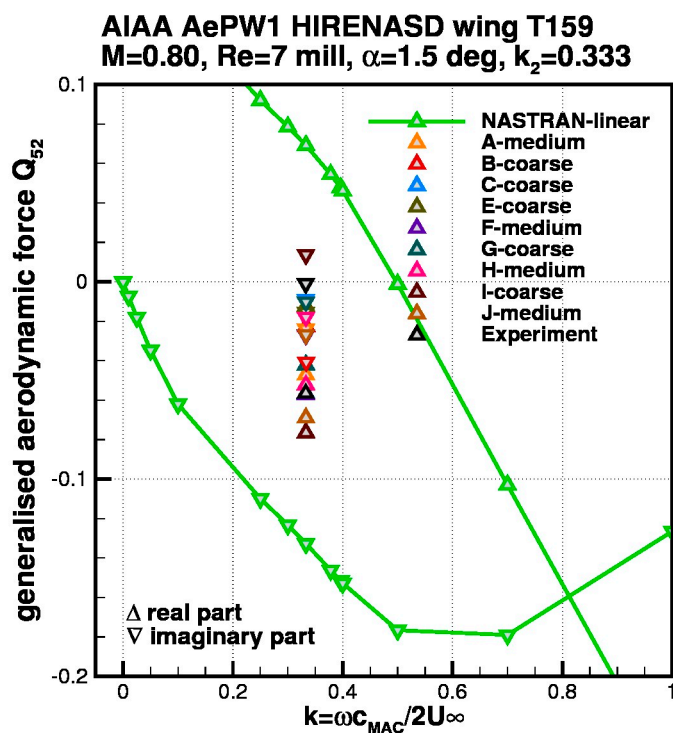


Figure 6-13 Comparison of computational results and experimental data for the representative results of all analysts, see also Table 1 (T159_Q52_med.jpg)

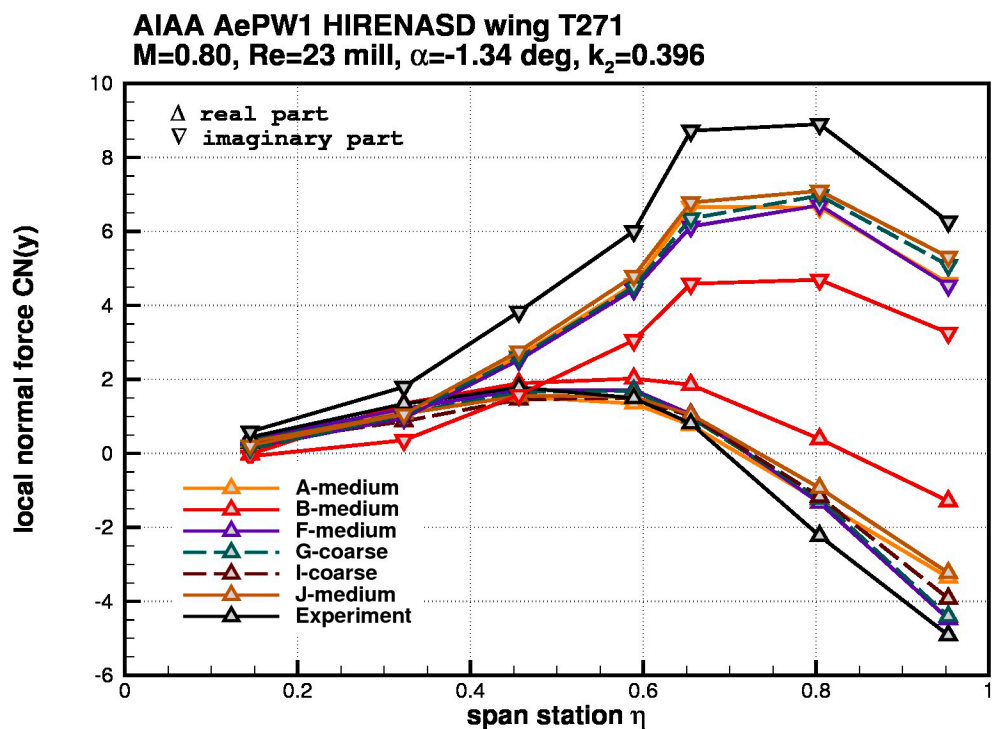


Figure 6-14 Comparison of computational results and experimental data for the representative results of all analysts, see also Table 1 (T271_CN_med.jpg)

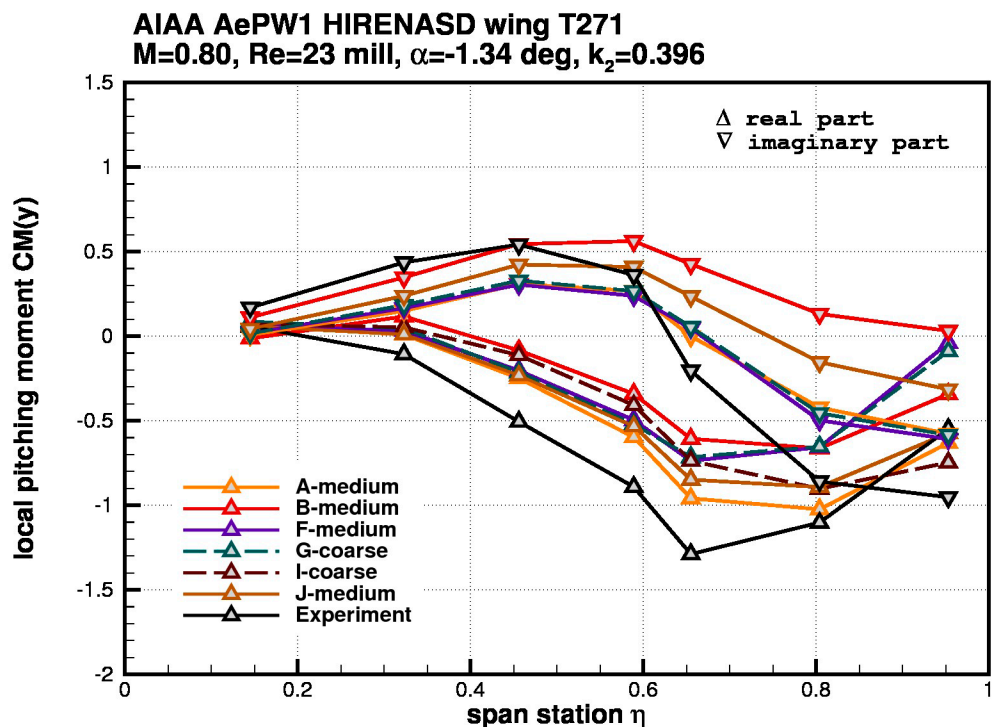


Figure 6-15 Comparison of computational results and experimental data for the representative results of all analysts, see also Table 1 (T271_CM_med.jpg)

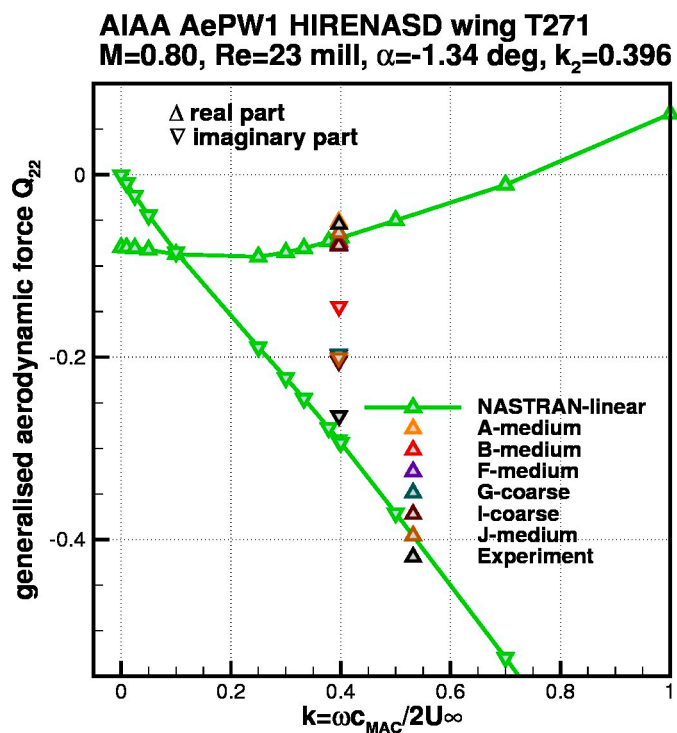


Figure 6-16 Comparison of computational results and experimental data for the representative results of all analysts, see also Table 1 (T271_Q22_med.jpg)

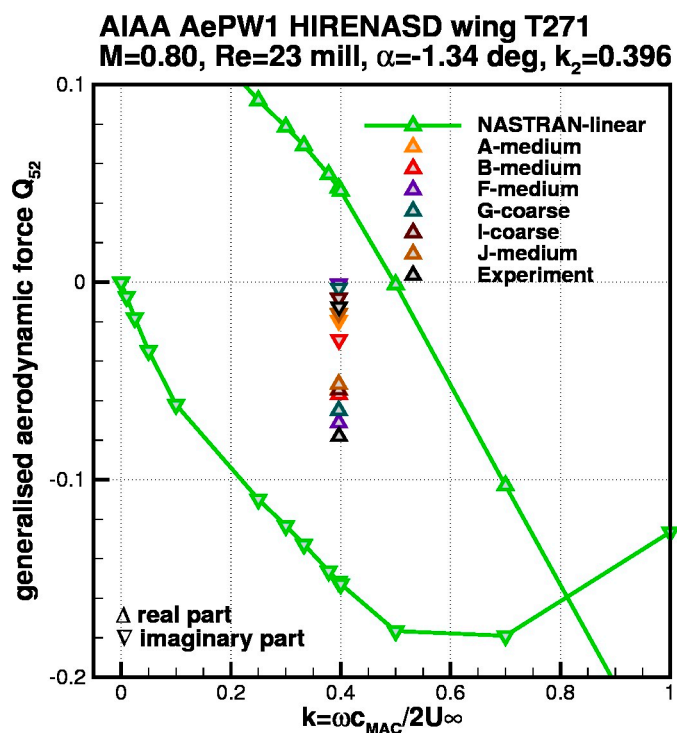


Figure 6-17 Comparison of computational results and experimental data for the representative results of all analysts, see also Table 1 (T271_Q52_med.jpg)